Chapter

High-Resolution Inelastic X-Ray Scattering: A Probe of Microscopic Density Fluctuations in Simple Fluids

Alessandro Cunsolo

Abstract

The explicit form of the inelastic X-ray scattering, IXS, cross-section is derived within a time-dependent perturbative treatment of the scattering process. In this derivation, the double differential cross-section is obtained from the Fermi Golden Rule within a plane wave expansion of the vector potential. Furthermore, it is assumed throughout that the Thompson term of the perturbative Hamiltonian yields the overwhelming contribution to the scattering. The achievement of an explicit form for the double differential scattering cross-section rests on the validity of the adiabatic or Born-Oppenheimer approximation. As a result, it is here shown that that the IXS double differential cross-section is proportional to the spectrum of density fluctuations of the sample, which is thus the sample variable directly accessed by IXS measurements. Although the whole treatment is valid for monatomic systems only, under suitable approximations, it can be extended to molecular systems.

Keywords: inelastic X-ray scattering, theory of the scattering, theory of the line-shape, double differential scattering cross-section

1. Introduction

Inelastic scattering measurements are among the most powerful tools to investigate the collective terahertz dynamics of disordered systems [1, 2]. Although this subject has been the focus of intense scrutiny in the past few decades, it still presents many challenging aspects. In a spectroscopic measurement, the dynamic response of the target system is stimulated via the exchange of an energy $\hbar\omega$ and momentum $\hbar\boldsymbol{Q}$ where $\hbar$ is the reduced Planck's constant. A suitable choice of the exchanged wavevector amplitude $Q = |\boldsymbol{Q}|$ and ω enables to tune the probe to dynamic events occurring over different scales. For infinitesimal Q and ω values, the measurement probes slowly decaying, hydrodynamic, density fluctuation modes either propagating or diffusing throughout the system, which resembles a continuous and homogeneous medium [3]. Upon increasing Q's and ω's, probed dynamic events become gradually faster and involve fewer atoms until the extreme, single-particle limit is reached. In this limit, the probe couples with the free recoil of

the single atom after the collision with the photon and before any interaction with the first neighboring atomic cage [4].

Although the spectral profile is exactly known analytically in both hydrodynamic and single-particle limits, its evolution at the crossover in between them still eludes a firm understanding. Particularly insightful appears the study of the lineshape in the mesoscopic range, which corresponds to $2\pi/Q$ and $2\pi/\omega$ values roughly matching nearest neighbor separations and 'in cage' rattling periods of atoms, respectively.

This range is the natural domain of high-resolution inelastic scattering, IXS [5], a spectroscopic method, which, since its development towards the end of the past millennium, has substantially improved the current understanding of the terahertz dynamics of condensed matter systems. This success partly owes to both inherent and practical advantages that this technique offers compared to the complementary terahertz spectroscopy, inelastic neutron scattering, INS. Intrinsic benefits include the virtual absence of kinematic limitations, the straightforward implementation of constant-Q energy scans, a mostly coherent cross-section and an often negligible multiple scattering contribution. More practical strengths are instead the substantially higher photon fluxes impinging on the sample and the smaller transversal size of the beam. However, these undoubted advantages can only be obtained at the cost of substantial count rate penalties. Indeed, the investigation of the collective dynamics in disordered systems imposes the access to energy transfer $E = \hbar\omega$ as low as a few meV. For IXS spectrometers, typically operated at $2.1\,10^4$ eV, resolving those energies imposes a resolving power of $\Delta E/E \leq 10^{-7}$. The achievement of such a challenging performance has held back for long the development of high-resolution IXS, which was only made possible by the advent of high-brilliance third-generation synchrotron sources and by parallel advances in the X-ray optics [6, 7].

As an introduction to the field, this chapter is devoted to a derivation of the cross-section of IXS measurements, thus elucidating its direct connection with the Fourier transform of the atomic density fluctuations autocorrelation function. A similar treatment, which can also be found in Refs. [5, 8], is strictly valid for monatomic systems only, even though it can be easily generalized to the case of molecular systems.

2. Generalities on an inelastic scattering measurement

In a typical IXS measurement, a beam of particles–waves, as, for example, neutrons, X-rays or electrons, having well-defined energy, wavevector and polarization impinges on a sample and, after the impact, it is scattered all over the solid angle. A detector placed at a distance r from the sample is used to count the particles deviated by an angle 2θ within the small solid angle $\Delta\Omega$ and intercepting its sensitive area $A = r^2\Delta\Omega$. Along the whole flight from the source to the detector, photons pass through optical elements filtering their energy both upstream and downstream of the sample, respectively referred to as monochromators and analysers. Other devices, such as collimators, mirrors, compound reflective lenses and so forth, are commonly used to shape the particle beam as required by experimental needs, and, specifically, they define its angular divergence and, whenever needed, its polarization.

At a long distance from the centre of the scattering, the electromagnetic wave generated by the scattering event is the sum of a plane and a spherical wave [9], that is, waves having respectively a planar and a spherical wavefront. In other terms, the ultimate effect of the scattering source is to remove a part of the photons from their

initial 'plane wave' state and reradiate them into a spherical wave, which is consistent with well-known Huygens-Fresnel principle [10]. However, it is always safe to assume that the detector—which intercepts photons deviated by an angle 2θ—has sensitive area $A = r^2\Delta\Omega$ small enough to safely approximate the spherical wave impinging on it as a plane wave. As a consequence, the scattering event probed in a real experiment can be portrayed as a transition of the photon states between two different plane waves, as schematically shown in **Figure 2**. These are characterized by well-defined wavevector $\boldsymbol{k}_{i,f}$ energy, $\hbar\omega_{i,f}$ and polarization $\hat{\varepsilon}_{i,f}$, with the indices 'i' and 'f' labelling the initial and final values, that is, the values before and after the scattering, respectively. Here all vector variables are indicated in bold.

As it appears from **Figure 1**, if one considers the plane defined by the two vectors $\boldsymbol{k}_i$ and $\boldsymbol{k}_f$, only one angular coordinate, the scattering angle 2θ, is sufficient to describe the scattering problem.

To derive an expression of the intensity detected in high-resolution *IXS* measurements, it is useful to recognize that these measurements are typically executed in transmission geometry, that is, by detecting the scattering signal downstream of the sample.[1]

For the sake of simplicity, a few more assumptions are here considered: (1) the sample has a straightforward shape: a slab of thickness t_s; (2) such a slab is crossed by the incident beam orthogonally to its front area; (3) the beam cross-section Σ_B is constant throughout the sample thickness, which implies that we are discarding the focusing of the incident beam; and (4) finally, for most *IXS* measurements, one can further assume that the beam only illuminates a limited portion of the whole cross-sectional area of the sample. However, the detector has a sensitive area sufficiently

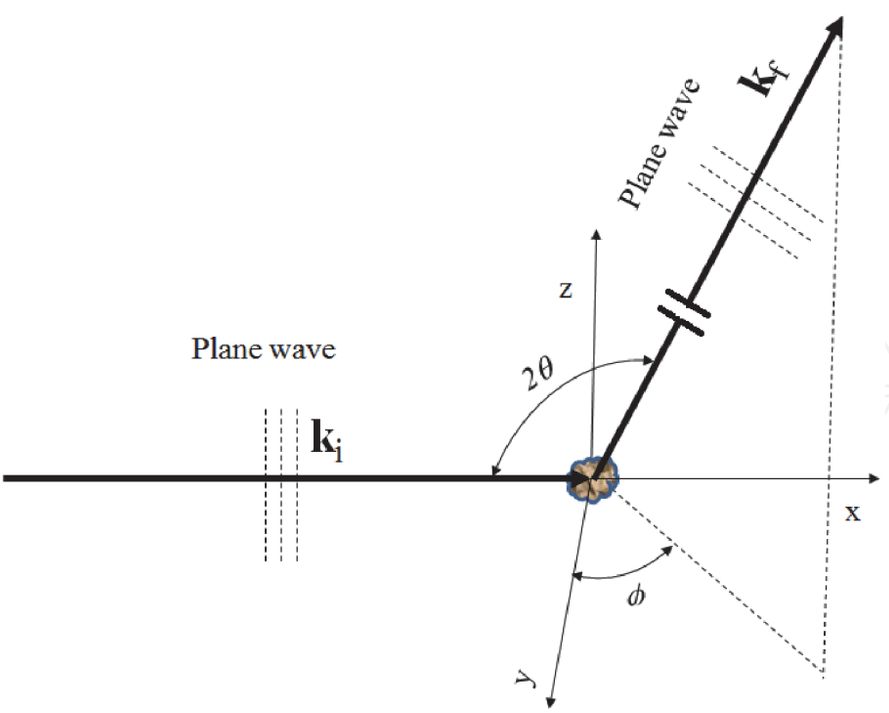

Figure 1.
A schematic rendering of the scattering process and the plane wave approximation (see text).

[1] For simple sample shapes, the treatment can be easily extended to the case of finite scattering angle by using simple trigonometry.

small, and a distance from the sample sufficiently large, that the scattered radiation impinging on it is schematizable as a plane wave, having wavevector $\boldsymbol{k}_f$ and wavefront perpendicular to it.

Under these assumptions, we can write a general expression to estimate the number of photons per unit time impinging on the detector, which is given by:

$$I \propto \Phi n_s \Sigma_B t_s \left(\frac{\partial^2 \sigma}{\partial \Omega \partial E_f} \right) \Delta\Omega dE_f, \tag{1}$$

where Φ is the photon flux on the sample, defined as the number of photons impinging on the sample per unit time and unit area, while n_s is the number of scattering units per unit volume, which is here assumed constant throughout the X-ray-illuminated sample.

The above formula introduces the double differential scattering cross-section:

$$\frac{d^2\sigma}{d\Omega \, \mathrm{d}E_f} = \frac{\begin{array}{c}\text{Rate of photons scattered into } d\Omega \text{ with} \\ \text{final energy between } E_f \text{ and } E_f + dE_f\end{array}}{\Phi d\Omega \, \mathrm{d}E_f}, \tag{2}$$

which is the only parameter of Eq. (1) conveying non-trivial information on the sample properties.

It can be recognized that the beam intensity across the sample thickness is not constant, as a part of it gets absorbed by the sample itself. This intensity reduction can be easily evaluated by expressing the attenuation caused by an elemental sample slice of thickness dx and located at a distance x. This intensity loss reads as:

$$dI = I(x + dx) - I(x) = -I\mu dx, \tag{3}$$

where μ is the absorption coefficient at the energy of the incident beam. The integration of both members of the above equation leads to the conclusion that the intensity transmitted through the sample experiences an exponential decay. Assuming a forward scattering geometry, the attenuation factor can be simply obtained as $exp\,(-\mu t_s)$ and inserted in Eq. (1), thus obtaining:

$$I = \Phi n_s \Sigma_B t_s \, exp\,(-\mu t_s) \left(\frac{\partial^2 \sigma}{\partial \Omega \partial E_f} \right) \Delta\Omega dE_{f.} \tag{4}$$

The above formula lends itself to a direct estimate of the ideal sample thickness, which is identified by the $\partial I / \partial t_s = 0$ condition, which yields $t_s = 1/\mu$. In summary, the optimal sample thickness should match the absorption length of the sample at the energy of the incident beam. For typical incident beam energies of most current *IXS* spectrometers, and for sample atomic species having electron number $Z > 4$, the extinction of the incident intensity is primarily caused by the photo-electric absorption process, which dominates over the Thomson scattering. The photoabsorption length typically decreases upon increasing *Z,* and this implies that *IXS* measurements on low Z materials require the use of relatively large samples, with a thickness in the *cm* range. However, this requirement becomes prohibitive for samples available in a small amount or that must be embedded in small volumes, as is typically the case of high-pressure experiments in Diamond Anvil Cells, *DACs*.

3. The interaction between impinging electromagnetic field and target electrons

Given this preliminary discussion, the focus is now on the analytical derivation of the *IXS* double differential cross-section $d^2\sigma/d\Omega dE_f$. An explicit analytical form requires, in the first place, a suitable expression for the Hamiltonian describing the interaction between the impinging photon beam and the electrons of the target sample. If one discards the relativistic nature of electron movements and neglects the usually weak contribution from the electron spin, such a Hamiltonian has the following form [5]:

$$H = \frac{1}{2M_e}\sum_i \left[\boldsymbol{p}_i - \frac{e}{c}\boldsymbol{A}(\boldsymbol{r}_i)\right]^2 + \sum_i V(\boldsymbol{r}_i) + V_{\text{int}}^{e-e}, \tag{5}$$

where $\boldsymbol{r}_i$ and $\boldsymbol{p}_i$ are the position and the momentum of the ith electron, respectively, V_{int}^{e-e} is the electron–electron interaction potential averaged over the electron clouds of target atoms, while $V(\boldsymbol{r}_i)$ is the potential acting on the ith electron. The above Hamiltonian can be cast in the following perturbative form:

$$H = H_{\text{el}} + H_{\text{int}}^{(1)} + H_{\text{int}}^{(2)}, \tag{6}$$

where the unperturbed Hamiltonian, associated with the multielectron system in the absence of the electromagnetic field, reads as:

$$H_{\text{el}} = \sum_i \left[\frac{p_i^2}{2M_e} + V(\boldsymbol{r}_i)\right] + V_{\text{int}}^{e-e}, \tag{7}$$

plus the other two terms accounting for the perturbation induced by the impinging electromagnetic field, that is, respectively:

$$H_{\text{int}}^{(1)} = \frac{-e}{2M_e c}\sum_i \{\boldsymbol{A}(\boldsymbol{r}_i), \boldsymbol{p}_i\} \tag{8}$$

and the so-called Thomson scattering term:

$$H_{\text{int}}^{(2)} = \frac{1}{2} r_0 \sum_i \boldsymbol{A}(\boldsymbol{r}_i)\cdot\boldsymbol{A}(\boldsymbol{r}_i). \tag{9}$$

Here the symbol $\{,\}$ denotes the anticommutator operator, while $r_0 = e^2/(M_e c^2)$ is the classical electron radius expressed in cgs units. To its leading order, the perturbation $H_{\text{int}}^{(1)}$ in Eq. (8) describes one-photon interactions with the sample as absorption and emission, while two-photon processes, such as the scattering event, come into play to the second-order only. Conversely, the Thomson term (Eq. (9)), being quadratic in the vector potential, accounts to the first order for two photons interactions such as the scattering event. Away from an energy resonance, the latter term largely exceeds the second-order expansion of Eq. (8), thus providing an overwhelming contribution to the scattering process, which will be hereafter assumed to be entirely described by the Thomson term.

As mentioned, in a typical scattering measurement, the X-ray photons undergo a transition between two different plane wave states. Therefore, one could, in principle, use the Fermi Golden Rule [11] to count all scattered photons emanating from a

single incident plane wave and having wavevector pointing to a 2θ direction to within a solid angle $\Delta\Omega$, thus deriving the double differential cross-section explicitly.

This strategy would require, in principle, a proper normalization of the photon wave functions, but, unfortunately, plane waves have normalization integral diverging for long distances. This difficulty is usually circumvented by confining the description of the scattering problem to a cubic box of size L and eventually considering the limit for large L. Within this L-sized cubic box, the vector potential becomes a linear combination of normalized plane waves which explicitly reads as [5]:

$$\boldsymbol{A}(\boldsymbol{r}) = \sum_{k,\alpha} \sqrt{\left(\frac{2\pi\hbar}{\omega_k L^3}\right)} c\hat{\varepsilon}_\alpha \left[a_{k,\alpha} \exp\left(i\boldsymbol{k}\cdot\boldsymbol{r}\right) + a^\dagger_{k,\alpha} \exp\left(-i\boldsymbol{k}\cdot\boldsymbol{r}\right)\right]. \tag{10}$$

Here the indexes 'k' and 'α' label, respectively, the wavevector and the polarization states of the wave; $a_{k,\alpha}$ and its Hermitian conjugate $a^\dagger_{k,\alpha}$ are the annihilation and creation operators, respectively; c is the speed of light in vacuum and ω_k is its angular frequency. Notice that the plus and minus signs in the phases of the exponential terms of Eq. (10) respectively define the upstream and downstream propagation of the photon plane wave.

Coming back to the double differential scattering cross-section, one can express it as:

$$\frac{d^2\sigma}{d\Omega dE_f} = \frac{dP_{i\to f}}{dt}\frac{1}{\Phi}\frac{d^2n}{d\Omega dE_f}, \tag{11}$$

where $dP_{i\to f}/dt$ is the probability rate per sample and probe units that a photon experiences a transition between the initial and the final photon states, while the term $d^2n/d\Omega dE_f$ represents the density of final photon states. The probability rate in Eq. (11) should be more appropriately written as a sum over all elementary excitations in the sample possibly coupling with the scattering event. Hence,

$$\frac{dP_{i\to f}}{dt} = \sum_{I,F} \frac{dP_{I,i\to F,f}}{dt}, \tag{12}$$

with $P_{I,i\to F,f}$ denoting the probability of a transition $|I,i\rangle \to |F,f\rangle$ between the combined states of the photon and the sample, labeled by lower case and capital fonts, respectively.

Eq. (12) is particularly useful as the term under summation can be derived explicitly using the Fermi Golden Rule, according to which:

$$\frac{dP_{I,i\to F,f}}{dt} = \frac{2\pi}{\hbar}\left(\frac{d^2n}{d\Omega dE_f}\right)|\langle F,f|H_{int}|I,i\rangle|^2. \tag{13}$$

The last factor in the right-hand side of the above equation contains the perturbative part of the Hamiltonian computed between initial and final combined photon and sample states. As mentioned, we will assume that this term entirely coincides with the Thomson term in Eq. (9).

At this stage, the derivation of the double differential cross-section requires one to tackle the density of final states $d^2n/d\Omega dE_f$ analytically, as discussed in the next paragraph.

4. Counting the photon states

It is worth noticing that the expedient of circumscribing the scattering within a L-sized cubic box, besides enabling a proper normalization of the plane waves, makes more straightforward the counting of the final state photon modes [11]. The number of plane waves with energy included between E_f and $E_f + dE_f$ and pointing to a direction 2θ within a solid angle $\Delta\Omega$ is given by:

$$\left(\frac{d^2n}{d\Omega dE_f}\right) dE_f \Delta\Omega. \tag{14}$$

In the reciprocal space, the bandwidth dE_f corresponds to the volume $dV(k_F)$ of the spherical shell of infinitesimal thickness represented in **Figure 2**, for which one can write $dV(k_f) = d\Omega k_f^2 dk_f$. The wavevectors' components in the box L representing the boundary of our scattering problem are:

$$k_x = (2\pi/L)n_x \;\; k_y = (2\pi/L)n_y \;\; k_z = (2\pi/L)n_z, \tag{15}$$

where n_x, n_y and n_z are generic integers.

The set of wavevectors defined in Eq. (15) identifies a lattice in k-space, whose simplest self-replicating unit cell has a volume $V_{\min} = (2\pi/L)^3$. If this volume is small enough—or, equivalently, if L is large enough—the number of lattice points within the elemental volume is given by the ratio $dV(k_f)/V_{\min}$ (**Figure 2**).

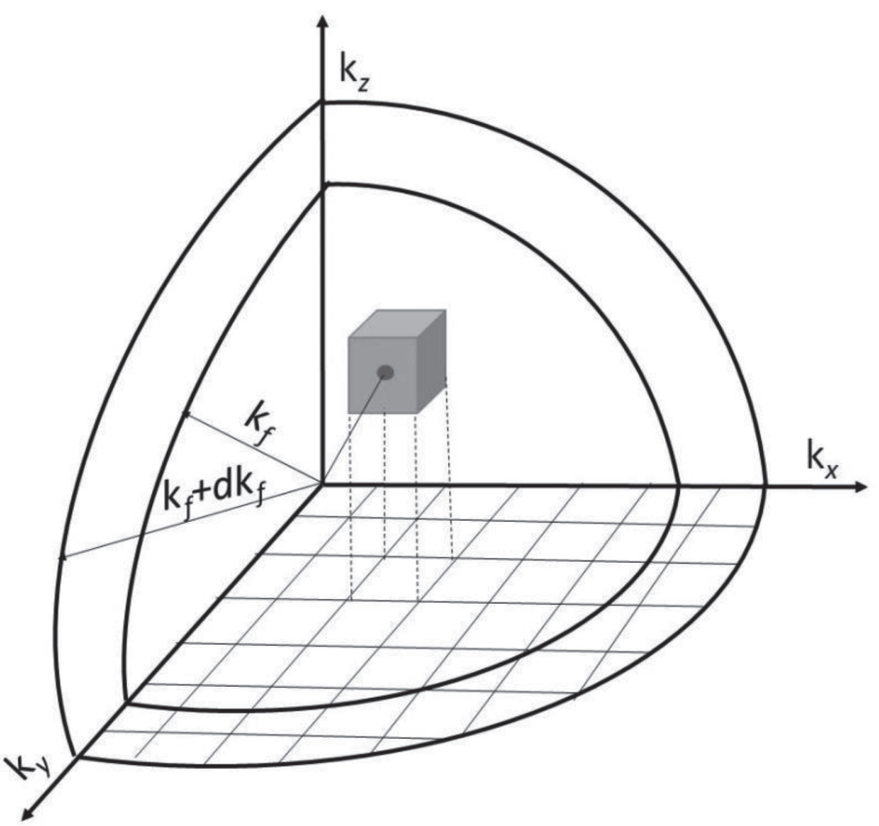

Figure 2.
The elemental volumes in the reciprocal space. Here the cube enclosing a lattice point represents the unit cell of size $V_{min} = (2\pi/L)^3$ (see text).

Therefore, one has

$$\left(\frac{d^2n}{d\Omega dE_f}\right)dE_f\Delta\Omega = k_f^2\left(\frac{L}{2\pi}\right)^3 dk_f d\Omega. \tag{16}$$

For photons, the link between energy and wavevector is fixed by the linear law $E_f = \hbar c k_f$, which can be differentiated to obtain $dE_f = \hbar c dk_f$, thus eventually getting

$$\left(\frac{d^2n}{d\Omega dE_f}\right)dE_f\Delta\Omega = \frac{k_f^2}{\hbar c}\left(\frac{L}{2\pi}\right)^3 dE_f d\Omega. \tag{17}$$

Therefore,

$$\frac{d^2n}{d\Omega dE_f} = \frac{L^3}{8\pi^2}\frac{k_f^2}{\hbar c}, \tag{18}$$

which, combined with Eq. (11), yields

$$\frac{d^2\sigma}{d\Omega dE_f} = \frac{L^3}{8\pi^2}\frac{k_f^2}{\hbar c}\frac{dP_{i\to f}}{dt}. \tag{19}$$

At this stage, the interaction term, that is, the squared matrix element appearing in the Fermi Golden Rule (Eq. (13)), can be made explicit by inserting in it the Thomson term in Eq. (9), while using the expression of the vector potential in Eq. (10), thus eventually obtaining

$$\sum_{j,m}\langle F|\, exp\left(-i\boldsymbol{Q}\cdot\boldsymbol{R}_j\right)|I\rangle\langle I|\, exp\left(i\boldsymbol{Q}\cdot\boldsymbol{R}_m\right)|F\rangle, \tag{20}$$

where the vector R_j is the position of the jth atom. The above formula embodies the momentum conservation law as it was derived assuming the identity $\hbar\boldsymbol{Q} = \hbar\left(\boldsymbol{k}_f - \boldsymbol{k}_i\right)$. Furthermore, when using Eq. (10), it was considered that $\omega(k)$ is equal to ck_i and ck_f in the initial and the final photon states, respectively. Combining all analytical steps illustrated above, one eventually obtains the following expression for the double differential cross-section:

$$\frac{\partial^2\sigma}{\partial\Omega\partial E_f} = r_0^2\frac{k_f}{k_i}\left(\hat{\varepsilon}_i\cdot\hat{\varepsilon}_f\right)^2 \times \sum_{F,I}P_I\left|\langle F|\sum_j exp\left(i\boldsymbol{Q}\cdot\boldsymbol{R}_j\right)|I\rangle\right|^2\delta(\hbar\omega + E_F - E_I). \tag{21}$$

Here, $\hbar\omega$ is the energy gained by the photons in the scattering process, while the δ-function term accounts for the energy conservation in the scattering process, as it ensures that $\hbar\omega = -(E_F - E_I)$ with $E_F - E_I$ being the energy gained by the sample. Notice that the cross-section defined above entails a sum over all states of the system, where the factor P_I represents the statistical population of the initial states of the sample.

5. From the adiabatic approximation to the dynamic structure factor

The right-hand side of Eq. (21) contains three independent factors, the integral term being the only one directly relating to the properties of the target sample. The

latter can hardly be handled analytically, due to the complex interplay between electrons belonging to different atoms, which couples electronic and nuclear coordinates. However, it becomes treatable under the reasonable approximation that the centre of mass of the electronic cloud drifts following with no delay the slow nuclear motion. This assumption is customarily referred to as 'adiabatic', or Born-Oppenheimer, approximation [11]; its use justifies the factorization of the target system 'ket' as $|S\rangle = |S_n\rangle|S_e\rangle$, with nuclear and electronic states being labeled by the suffixes 'n' and 'e' respectively. The accuracy of this assumption ultimately owes to the substantially different nuclear and electronic masses and the correspondingly different timescales defining their dynamics. It holds validity when the energy exchange is smaller than all excitation energies of electrons in bound core states, which includes all cases of practical interest for this book. With $|S_e\rangle$ being unaffected by the scattering process, the difference between the initial $|I\rangle = |I_n\rangle|I_e\rangle$ and the final $|F\rangle = |F_n\rangle|F_e\rangle$ states of the sample is uniquely due to excitations associated with atomic density fluctuations.

Within the validity of these assumptions, the double differential cross-section in Eq. (18) reduces to

$$\frac{\partial^2\sigma}{\partial\Omega\partial E_f} = r_0^2\frac{k_f}{k_i}\left(\hat{\varepsilon}_i\cdot\hat{\varepsilon}_f\right)^2\sum_{F_n,I_n}P_{I_n}\left|\langle F_n|\sum_j f_j(\boldsymbol{Q})\,exp\left(i\boldsymbol{Q}\cdot\boldsymbol{R}_j\right)|I_n\rangle\right|^2\times\delta(\hbar\omega+E_{F_n}-E_{I_n}), \tag{22}$$

where E_{I_n} and E_{F_n} are the energies associated with the initial and final nuclear states respectively, and

$$f_j(\boldsymbol{Q}) = \langle F_e|\sum_{\alpha=1}^{Z} exp\left(i\boldsymbol{Q}\cdot\boldsymbol{r}_\alpha^j\right)|I_e\rangle \tag{23}$$

is the form factor of the jth atom. Here r_α^j is the coordinate of the αth electron in the centre of mass frame of the jth atom, while $|I_e\rangle$ coincides with the ground state of the electronic wave function of a given atomic nucleus. In practice, $f(\boldsymbol{Q})$ can be approximated by the value calculated for a free atom, that is, in the perfect gas phase, as the electronic cloud distribution is essentially unchanged upon phase transition. The primary contribution to this factor comes from core electrons whose orbits are more tightly bound to the much more massive atomic nucleus.

If a single atomic species is present in the sample, all atoms have the same form factor, that is, $f_j(\boldsymbol{Q}) \equiv f(\boldsymbol{Q})$; this further simplifies the expression of the double differential cross-section

$$\frac{\partial^2\sigma}{\partial\Omega\partial E_f} = K\sum_{F_n,I_n}P_{I_n}\left|\langle F_n|\sum_m exp\left(i\boldsymbol{Q}\cdot\boldsymbol{R}_m\right)|I_n\rangle\right|^2\delta(\hbar\omega+E_{F_n}-E_{I_n}) \tag{24}$$

where $K = r_0^2\frac{k_f}{k_i}\left(\hat{\varepsilon}_i\cdot\hat{\varepsilon}_f\right)^2|f(\boldsymbol{Q})|^2$.

The above expression can be cast in a more compact form after the few additional manipulations as the use of an integral representation of the δ-function of energy, the Heisenberg representation of a time-dependent operator and the completeness of the final eigenstate.

In its initial state, the sample is usually a many-atoms system at equilibrium, and the sum over its initial state can be computed as an ordinary equilibrium average, which leads to the following identity:

$$\sum_{I_n} P_{I_n} \langle I_n | \exp\left[-i\boldsymbol{Q}\cdot\boldsymbol{R}_k(0)\right] \exp\left[i\boldsymbol{Q}\cdot\boldsymbol{R}_j(t)\right] | I_n \rangle = \sum_{k,j} \langle \exp\left[-i\boldsymbol{Q}\cdot\boldsymbol{R}_k(0)\right] \exp\left[i\boldsymbol{Q}\cdot\boldsymbol{R}_j(t)\right] \rangle, \tag{25}$$

where as usual, the angle brackets $\langle \ldots \rangle$ denote the thermal average on the system at equilibrium. The expression above is the time correlation function of the variable $\sum_j exp\left[-i\boldsymbol{Q}\cdot\boldsymbol{R}_j(t)\right]$, which involves the pair composed by the jth and kth atoms. The physical meaning of this variable will be discussed in the next section in further detail.

In summary, as a result of all manipulations mentioned above, the double differential cross-section in Eq. (24) eventually reduces to

$$\frac{\partial^2\sigma}{\partial\Omega\partial E_f} = \frac{K}{2\pi\hbar}\int_{-\infty}^{\infty} dt \langle \sum_{j=1}^{N}\sum_{k=1}^{N} \exp\left\{i\boldsymbol{Q}\cdot\left[\boldsymbol{R}_j(t)-\boldsymbol{R}_k\right]\right\}\rangle \exp\left(-i\omega t\right) \tag{26}$$

where $\boldsymbol{R}_k$ is the shorthand notation for $\boldsymbol{R}_k(0)$.

6. Introducing a key stochastic variable: the microscopic density fluctuation

The expression between angle brackets is the equilibrium autocorrelation function of the dynamic variable $n(\boldsymbol{Q},t) = \sum_j \exp\left[i\boldsymbol{Q}\cdot\boldsymbol{R}_j(t)\right]$, which involves the positions of the generic kth and kth atom pair, that is, $\boldsymbol{R}_k(t)$ and $\boldsymbol{R}_j(0)$ respectively, evaluated at different times. The variable $n(\boldsymbol{Q},t)$ is the Fourier transform of the microscopic number density of the system, which, for a system of N atoms is defined as:

$$n(\boldsymbol{r},t) = \sum_{j=1}^{N} \delta\left[\boldsymbol{r}-\boldsymbol{R}_j(t)\right]. \tag{27}$$

The interpretation of this function as a microscopic density is perhaps more evident as one considers its average value over the whole sample volume:

$$n = 1/V\int_V d\boldsymbol{r} n(\boldsymbol{r},t) = 1/V\int_V d\boldsymbol{r}\sum_{j=1}^{N}\delta\left[\boldsymbol{r}-\boldsymbol{R}_j(t)\right] = N/V, \tag{28}$$

which is consistent with the macroscopic definition of number density. Notice that the δ-function is an extremely irregular discontinuous profile, which however adequately accounts for the atomistic, character of the system.

In the reciprocal space, one deals with the Fourier transform of the microscopic density, namely

$$n(\boldsymbol{Q},t) = \int_V d\boldsymbol{r}\left\{\sum_{j=1}^{N}\delta\left[\boldsymbol{r}-\boldsymbol{R}_j(t)\right]\right\} exp\left(i\boldsymbol{Q}\cdot\boldsymbol{r}\right) = \sum_{j=1}^{N} exp\left[i\boldsymbol{Q}\cdot\boldsymbol{R}_j(t)\right]. \tag{29}$$

Furthermore, since scattering phenomena arise from inhomogeneities or fluctuation from equilibrium, we are here mainly interested in the microscopic density fluctuation:

$$\delta n(\boldsymbol{r},t) = \sum_{j=1}^{N}\delta\left[\boldsymbol{r}-\boldsymbol{R}_j(t)\right] - n, \tag{30}$$

Again, the variable of direct pertinence for a spectroscopic measurement is instead the Fourier transform of such a fluctuation:

$$\delta n(\boldsymbol{Q},t) = \sum_{j=1}^{N} exp\left[i\boldsymbol{Q}\cdot\boldsymbol{R}_j(t)\right] - n\delta(\boldsymbol{Q}); \tag{31}$$

in which it was considered that the Fourier transform of a constant function is a δ-function.

We can now introduce the intermediate scattering function as the space Fourier transform of the correlation function between density fluctuations:

$$F(\boldsymbol{Q},t) = \frac{1}{N}\int_V d\boldsymbol{r}\langle\delta n(\boldsymbol{r},t)\delta n(\boldsymbol{r},0)\rangle\, exp\,(i\boldsymbol{Q}\cdot\boldsymbol{r}) \tag{32}$$

and its one-sided time Fourier transform

$$S(\boldsymbol{Q},\omega) = \frac{1}{2\pi\hbar}\int_0^{\infty} dt\, F(\boldsymbol{Q},t)\, exp\,(-i\omega t), \tag{33}$$

which is customarily referred to as the spectrum of density fluctuations, or the dynamic structure factor of the system.

7. The double differential cross-section and the dynamic structure factor

Given the dynamic variables introduced in the previous section, it can be readily verified that Eq. (26) can be cast in the more compact form:

$$\frac{d^2\sigma}{d\Omega dE_f} = N\frac{r_0^2}{\hbar}\left(\frac{k_f}{k_i}\right)\left(\hat{\varepsilon}_i\cdot\hat{\varepsilon}_f\right)^2|f(Q)|^2 S_n(Q,\omega), \tag{34}$$

where

$$S_n(Q,\omega) = \frac{1}{2\pi\hbar N}\int_{-\infty}^{+\infty} dt\langle n(\boldsymbol{Q},0)n(\boldsymbol{Q},t)\rangle\, exp\,(-i\omega t) \tag{35}$$

is the spectrum associated with the dynamic variable $n(\boldsymbol{Q},t)$. Notice that for a homogeneous and isotropic system such as a liquid, such a variable does not depend on the direction of the exchanged wavevector, but uniquely on its amplitude $Q = |\boldsymbol{Q}|$.

Let us discuss here how the spectrum in Eq. (35) relates to the variable density fluctuations as defined by Eq. (30). By definition, the spectrum of such a variable is the Fourier transform of the autocorrelation function. Explicitly

$$\begin{aligned} S_{\delta n}(Q,\omega) &= \frac{1}{2\pi\hbar N}\int_{-\infty}^{\infty} dt\langle\delta n(\boldsymbol{Q},t)\delta n(\boldsymbol{Q},0)\rangle\, exp\,(-i\omega t) \\ &= \frac{1}{2\pi\hbar N}\int_{-\infty}^{\infty} dt\langle n(\boldsymbol{Q},t)n(\boldsymbol{Q},0)\rangle\, exp\,(-i\omega t) + C\delta(\omega)\delta(\boldsymbol{Q}), \end{aligned} \tag{36}$$

with $C = n^2/\hbar N$. At this stage, one can define the spectrum of the microscopic density as

$$S_n(Q,\omega) = S_{\delta n}(Q,\omega) + n^2\delta(\omega)\delta(\mathbf{Q}). \tag{37}$$

It appears that the spectra of either $n(\mathbf{Q},t)$ or $\delta n(\mathbf{Q},t)$, which are labeled by the respective indexes n and δn, differ by a term proportional to the product $\delta(\omega)\delta(Q)$.

This term accounts for the forward transmitted elastic scattering, which is of no relevance for a scattering experiment as it describes the signal from photons that have exchanged no energy or momentum with the target sample.

In practice, such a signal is never detected by scattering measurements, as it does not convey insight into non-trivial samples properties; furthermore, it fully overlaps with the forward transmitted beam, which is often so intense to burn or damage detectors. For these reasons, IXS measurements are always performed at finite scattering angles, where one has

$$S_n(Q,\omega) = S_{\delta n}(Q,\omega) \equiv S(Q,\omega), \tag{38}$$

with

$$S(Q,\omega) = \frac{1}{2\pi N}\int_{-\infty}^{+\infty} dt\langle\delta n(\mathbf{Q},0)\delta n(\mathbf{Q},t)\rangle\, exp\,(-i\omega t), \tag{39}$$

As discussed, the identity above entails the replacement of the microscopic density $n(\mathbf{Q},t)$ with its fluctuation from equilibrium $\delta n(Q,t)$

$$\frac{d^2\sigma}{d\Omega dE_f} = KS(Q,\omega), \tag{40}$$

where $K = N\left(r_0^2/h\right)\left(k_f/k_i\right)\left(\hat{\varepsilon}_i\cdot\hat{\varepsilon}_f\right)^2|f(Q)|^2$.

This expression of the cross-section above has been derived assuming a target sample composed by N identical atoms and within the Born-Oppenheimer approximation. When different atomic species are present in the sample, within the validity of the Born-Oppenheimer approximation, the derivation of the scattering cross-section is similar, provided the system is isotropic, that is, invariant under rotations, and a weak coupling exists between molecular rotations and centre of mass movements. The 'effective' form factor, in this case, results from the average value of the form factors of different atoms in the molecule. The general case, of a system composed of molecules with a pronounced anisotropy, that is, a markedly non-spherical shape, makes the computation of the cross-section slightly more complicated.

A more detailed treatment of this problem within the hypothesis of random molecular orientations and weak coupling between orientational and translational degrees of freedom leads to the conclusion that the spectrum splits into a coherent and an incoherent component. Consequently, the cross-section can be cast in the following general form:

$$\frac{\partial^2\sigma}{\partial\Omega\partial\omega} = A\left\{\langle F^2(Q)\rangle_\Omega S_C(Q,\omega) + \delta\langle F^2(Q)\rangle_\Omega S_I(Q,\omega)\right\} \tag{41}$$

where $\delta\langle F(Q)^2\rangle_\Omega = \langle F(Q)^2\rangle_\Omega - \langle F(Q)\rangle_\Omega^2$, where the suffix '$\Omega$' indicates an average over molecular orientations, while the suffixes 'I' and 'C' label the incoherent and coherent parts of the dynamic structure factor.

8. An estimate of the count rate

An estimate of the count rate achievable by an IXS measurement can be worked out starting from the expression of the total scattering cross-section, while assuming, for instance, a sample having an optimal thickness $t_s = 1/\mu$. The flux of scattered photons in the solid angle $\Delta\Omega$ and the energy interval ΔE_f is thus given by

$$d\dot{N} = \dot{N}_0 \, exp\,(-1)\frac{n_s}{\mu}\frac{d^2\sigma}{d\Omega dE_f}\Delta\Omega\Delta E_f. \tag{42}$$

At this stage, both members of the equation can be integrated in time, and the double integration over both solid angle and final energy must also be performed to obtain the total cross-section of the IXS scattering. In the low Q limit, where the atomic form factor $f(Q) \approx Z$ and that the approximation $\left(k_f/k_i\right)\left(\hat{\varepsilon}_i \cdot \hat{\varepsilon}_f\right)^2 = 1$, one has:

$$\frac{N}{N_0} \propto \frac{(Zr_0)^2 n_s}{\mu} = \frac{\sigma_C}{\sigma_A}, \tag{43}$$

where $\sigma_C = (Zr_0)^2$, while $\sigma_A = n_s/\mu$ is the absorption cross-section. An idea of the counting efficiency of IXS is provided by **Figure 3**, which displays the value of the σ_C/σ_A ratio for an incident X-ray beam having 10 keV energy, as a function of the atomic number. The abrupt increase of this parameter can be readily appreciated at the absorption above the K-edge, that is, above the binding energy of the innermost electron shell; these innermost electrons are those primarily interacting with the incident X-ray.

8.1 The signal measured by a real instrument

As a result of the previous treatment, it was demonstrated that the cross-section is proportional to $S(Q, \omega)$. However, such a treatment is entirely classical, insofar as

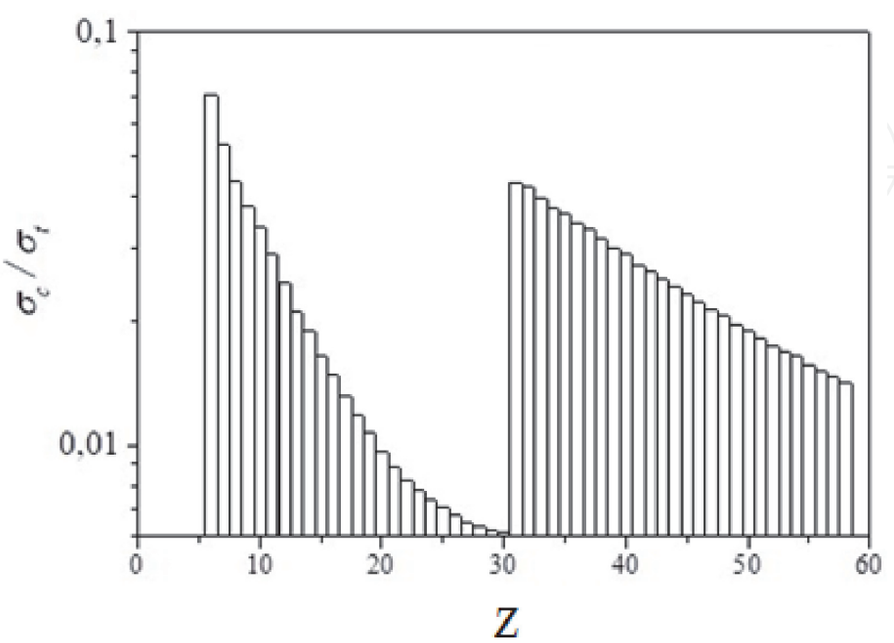

Figure 3.
The cross-sections ratio defined in Eq. (45) is reported as a function of the atomic number Z, for a 10 keV energy X-ray beam (courtesy of F. Sette).

all relevant observables are treated as commuting variables. Quantum effects are accounted for only through the so-called detailed balance principle, which takes into account the statistical population of the various $\hbar\omega$-states of the sample. These effects ultimately result in an asymmetry of the spectrum respect to its elastic, $\hbar\omega = 0$, position. The most popular recipe for handling them is to assume that the true spectrum $\tilde{S}(Q,\omega)$ can be obtained from the classic, symmetric, counterpart $S(Q,\omega)$ by adding a suitable frequency-dependent factor. Explicitly,

$$\tilde{S}(Q,\omega) = \frac{\hbar\omega}{k_B T}\left[\frac{1}{1 - exp\,(-\hbar\omega/k_B T)}\right] S(Q,\omega). \tag{44}$$

Still, the above formula does not capture two essential aspects of the measured scattering signal, as the contribution of the instrumental resolution and the spectral background. These are explicitly accounted for by using the following general expression for the intensity profile:

$$I = I(Q,\omega) = A\left[\tilde{S}(Q,\omega) \otimes R(\omega)\right] + B(\omega) \tag{45}$$

where A is an overall intensity factor, while the usually mildly frequency-dependent coefficient $B(\omega)$ accounts in principle for both the spectral background

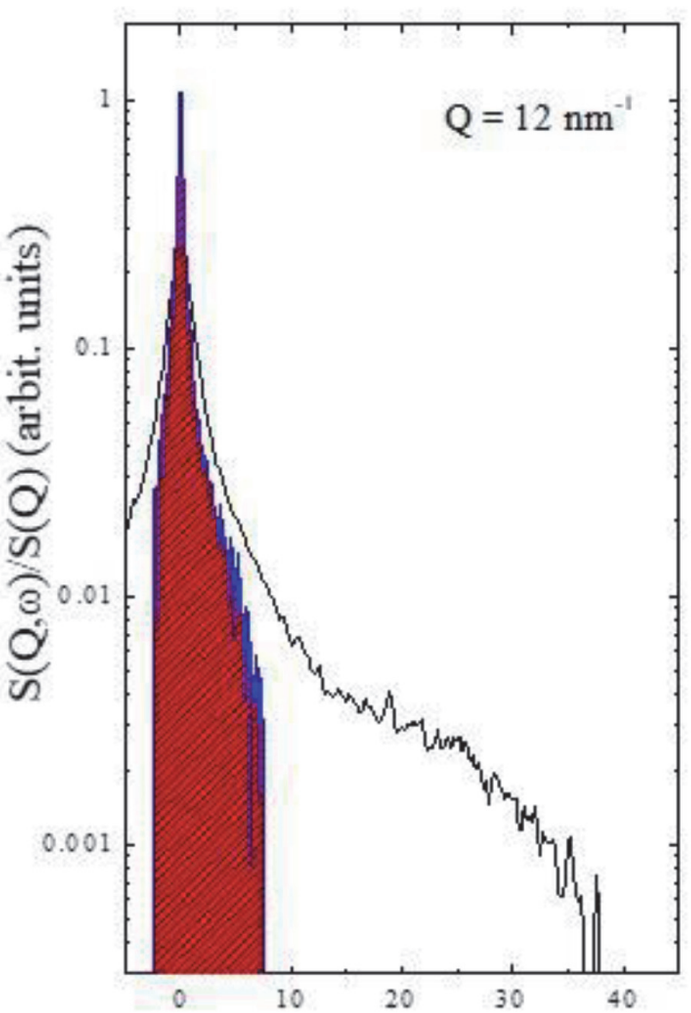

Figure 4.
The spectral line-shapes measured by IXS (black line) and INS (shadowed blue line) on a D_2O sample at ambient conditions. The spectra are reported after rescaling to the respective integrated intensities. Data are redrawn from ref. notice the remarkable difference in the explored ω-range. Data are redrawn from Ref. [13].

and the dark counts of a detector; when modeling the line-shape, sometimes the latter coefficient is assumed either constant or linearly dependent on ω.

The resolution profile represents the instrumental rendering of a spectral shape having zero energy width, that is, the $\delta(\omega)$–profile representing a perfectly elastic scattering. In a typical IXS measurement, such a resolution is estimated by measuring the scattering signal from an almost perfect elastic scatterer, often identified in a sample of plexiglas at the Q-position of the first sharp diffraction peak.

8.2 A practical example: a comparison between an IXS and an INS measurement

In general, the kinematic laws ruling the scattering process impose some limitations to the dynamic Q,ω region explorable by the measurement. These kinematic constraints are especially severe for inelastic neutron scattering, INS [2]. Although these limitations are irrelevant for IXS, the portion of the dynamic plane explored by this technique is still limited in the low-energy, or low-frequency, side by the finite instrumental energy resolution.

Figure 4 provides a clear example of how resolution and kinematic limitations differently affect IXS and INS. Indeed, the plot compares the spectra measured in a joint INS and IXS measurement on the same sample of heavy water [12], after normalization of the respective areas. The elastic peak in the INS spectrum has a spike-like shape. Such a sharp shape could be measured thanks to the 0.08 meV broad Gaussian resolution function. Which enables a superior definition of the spectral shape. However, this performance imposes an overall shrinkage of the spanned frequency range, which does not include the high-frequency shoulder in the IXS spectrum. On the other hand, the resolution of the IXS measurement is too coarse to enable a proper definition of the quasielastic portion of the scattering profile.

9. Conclusion

In conclusion, we illustrated the main analytical steps leading to a derivation of the inelastic X-ray scattering, IXS signal, and demonstrated its direct link with the terahertz spectrum of atomic density fluctuations.

Since its development in the mid-1990s, high-resolution IXS has rapidly transitioned to its mature age, nowadays representing an essential tool to characterize the terahertz dynamics of liquid and amorphous materials. Historically, the mainstream scientific interest of the IXS community was mostly limited to simple fluids and glass-forming materials. In recent years, such a focus has gradually shifted towards nanostructured metamaterials and biological systems. Since the high complexity of these systems often challenges a firm understanding of the measurement outcome, a firm theoretical modeling of the IXS signal from these highly heterogeneous systems would be highly beneficial.

Acknowledgements

This work used resources of the National Synchrotron Light Source II, a U.S. Department of Energy Office of Science User Facility operated for the DOE Office of Science by Brookhaven National Laboratory under Contract No. DE-SC0012704.

Author details

Alessandro Cunsolo
National Synchrotron Light Source-II, Brookhaven National Laboratory, Upton, NY, USA

*Address all correspondence to: acunsolo@bnl.gov

IntechOpen

References

[1] Lovesey SW. Theory of Neutron Scattering from Condensed Matter. Oxford: Oxford University Press; 1984

[2] Squires GL. Introduction to the Theory of Thermal Neutron Scattering. Cambridge: Cambridge University Press; 1978

[3] Berne BJ, Pecora R. Dynamic Light Scattering. New York: Wiley; 1976

[4] Silver RN, Sokol PE. Momentum Distributions. New York: Springer Science; 1989

[5] Sinha SK. Theory of inelastic X-ray scattering from condensed matter. Journal of Physics. Condensed Matter. 2001;**13**:7511-7523. DOI: 10.1088/0953-8984/13/34/304

[6] Masciovecchio C, Bergmann U, Krisch M, Ruocco G, Sette F, Verbeni R. A perfect crystal X-ray analyzer with 1.5 meV energy resolution. Nuclear Instruments and Methods in Physics Research. 1996;**117**:339-340. DOI: 10.1016/0168-583X(96)00334-5

[7] Verbeni R, Sette F, Krisch MH, Bergmann U, Gorges B, Halcoussis C, et al. X-ray monochromator with 2×10^8 energy resolution. Journal of Synchrotron Radiation. 1996;**3**:62-64. DOI: 10.1107/S0909049595015883

[8] Scopigno T, Ruocco G, Sette F. Microscopic dynamics in liquid metals: The experimental point of view. Reviews of Modern Physics. 2005;**77**:881-933. DOI: 10.1103/RevModPhys.77.881

[9] Jackson JD. Classical Electrodynamics. New York: Wiley; 1999

[10] Born M, Wolf E. Principles of Optics: Electromagnetic Theory of Propagation, Interference and Diffraction of Light. Cambridge: Cambridge University Press; 1999

[11] Bransden BH, Joachain CJ. Physics of Atoms and Molecules. Harlow: Pearson Education; 2003

[12] Balucani U, Zoppi M. Dynamics of the Liquid State. Oxford: Oxford University Press; 1994

[13] Cunsolo A, Kodituwakku CN, Bencivenga F, Frontzek M, Leu BM, Said AH. Transverse dynamics of water across the melting point: A parallel neutron and X-ray inelastic scattering study. Physical Review B. 2012;**85**:174305. DOI: 10.1103/PhysRevB.85.174305